Application Note #157

Webinar Recap: A Guided Tour of AFM Modes for Materials Characterization

The hundreds of modes + probes combinations available today provide endless opportunities for AFM studies in materials research. In this webinar, Bruker AFM experts reviewed modes ranging from the foundational to the specialized. They presented case studies for four different application spaces: polymers, semiconductors, battery technology, and 2D materials.

Webinar Presenters:
Ian Armstrong, Ph.D.
Peter De Wolf, Ph.D.
John Thornton, Ph.D.
Ravi Chintala, Ph.D.
Senli Guo, Ph.D.

Modes 101

At the hub of the AFM modes "wheel" – as Application Manager Ian Armstrong calls it – are the primary topographical modes. These include contact mode, TappingMode™, Fast Scanning, as well as Bruker's exclusive PeakForce Tapping®. Extending beyond topographical imaging are the spokes of the wheel, the secondary or derivative modes. While many secondary modes exist, they all generally fall into the categories of: electrical, mechanical, thermal, electrochemical, chemical, and fabrication. As a bonus, all these modes can be performed in a variety of environmental conditions: in a glove box, heated or cooled, with controlled humidity, or in a controlled atmosphere.

In this webinar, our webinar hosts gave **22 specific case study examples** of AFM modes used in several important applications in materials research and industry.

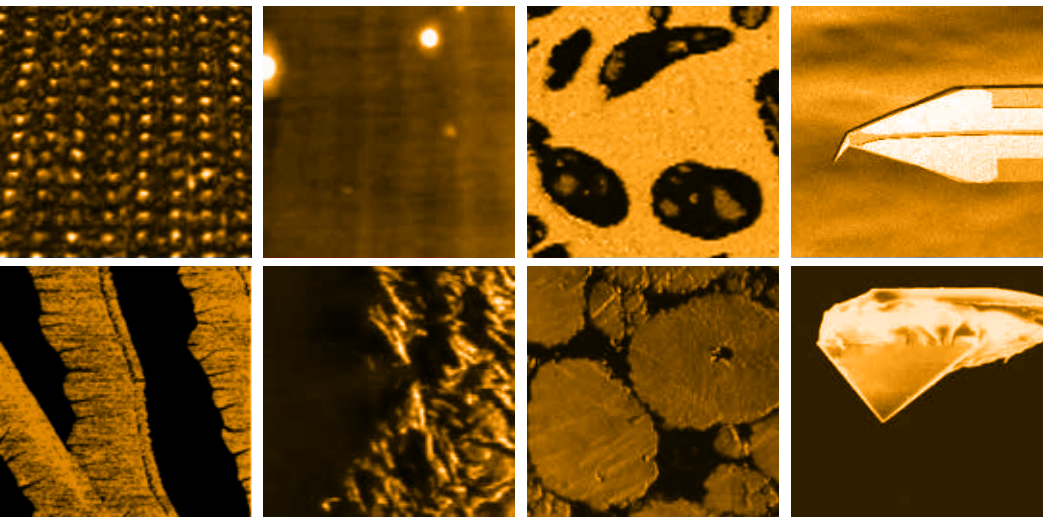

FIGURE 1.

Collection of AFM application and probe tip images.

Polymers

Dr. Thornton presented four different polymer case studies:

1. Nanomechanical and nanochemical characterization of impact modified copolymers
   PeakForce QNM®, AFM-nDMA, and AFM-IR were used to conduct nanoscale property mapping on impact modified copolymers [1,2]. These modes provide insights into the distribution of individual copolymer components and provide quantitative measurements of the resulting elastic, viscoelastic, and chemical properties.

2. Temperature studies of PHB/V crystallization
   Fast scanning was used to directly observe in situ crystallization of Poly(3-hydroxybutyrate-co-3-hydroxyvalerate) (PHB/V) in real-time. Varying the temperature of the sample resulted in changes to both the crystal structure and growth dynamics. Related publications can be found at [3,4].

3. Thermal analysis of multilayer packaging material
   Using the AFM tip to induce localized heating, nanoscale thermal analysis (nanoTA) was conducted on a cross-sectioned multilayer packaging material, seen in Figure 2. At each location, melting temperature of the component of interest was determined by identifying when the tip deflected into the sample, without needing to heat the bulk of the sample.

4. Electrical measurements on P3HT thin films with conductive fibers
   PeakForce TUNA™ was a key technique used to relate charge transport in Poly(3-Hexylthiophene) (P3HT) directly to its multiscale ordered structure [5].

MODES
Terminology

PeakForce QNM
– PeakForce Quantitative Nanomechanical Mapping

AFM-nDMA
– AFM Nanoscale Dynamic Mechanical Analysis

AFM-IR
– Atomic Force Microscopy-Based Infrared Spectroscopy

nanoTA
– Nanoscale Thermal Analysis

TUNA
– Tunneling AFM

C-AFM
– Conductive AFM

SCM
– Scanning Capacitance Microscopy

KPFM
– Kelvin Probe Force Microscopy

sMIM
– Scanning Microwave Impedance Microscopy

FIGURE 2.

Polymer multilayer packaging material, analyzed using nanoTA to determine local melting temperature of layers and interfaces.

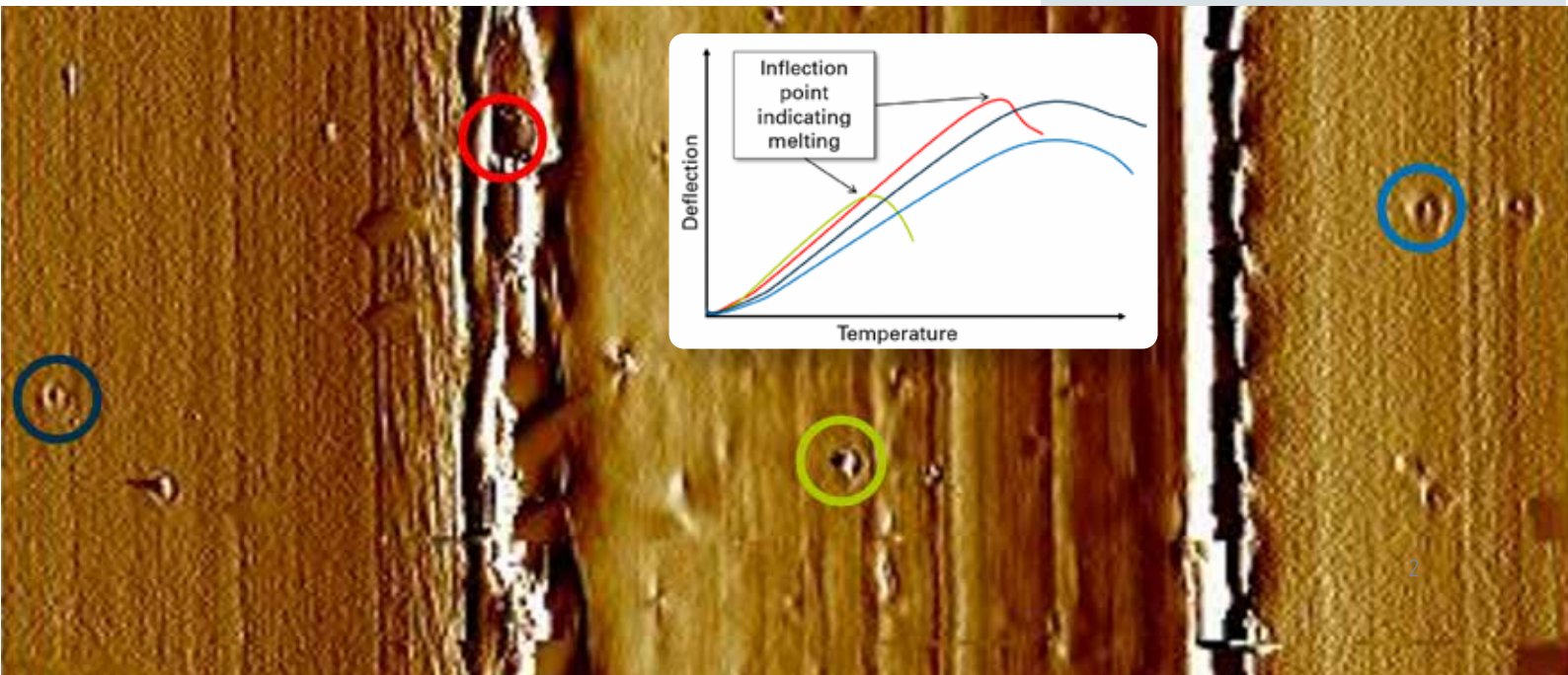

Semiconductors

Dr. Chintala presented how various nanoelectrical AFM modes are used to study semiconductor materials and devices.

1. Organic photovoltaic material
   Variations in local conductivity measured by C-AFM™ revealed phase separation of the components within the material. Current maps (e.g., Figure 3, right) are an indirect indicator of the chemical nature of the sample.

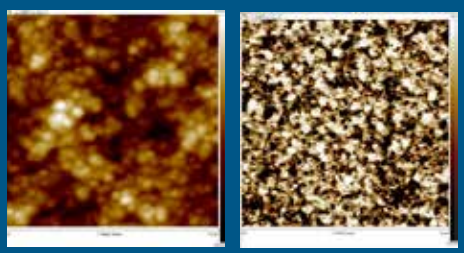

FIGURE 3.

Conductive AFM enables high-resolution current mapping that directly correlates to topgraphical data in this organic photovoltaic material.

2. Device failure analysis
   Deposited metal contacts on a device surface were imaged by C-AFM. The resulting conductivity map revealed differences in the quality/consistency of the contacts. I-V spectra were then collected on individual contacts which provided localized, quantitative measurements of their conductivity.

3. Defect characterization
   Defects in the SiO_2 layer of a silicon-based device were imaged using TUNA mode in constant current mode (where the feedback loop maintains a constant current by adjusting the applied voltage). Areas of lower voltage indicate the presence of a defect in the oxide layer. Supplemental TEM imaging showed that this defect was the result of oxide thinning.

4. Dopant carrier profiling
   Using scanning capacitance microscopy (SCM), the carrier type and concentration were assessed through the cross section of a 70 nm dopant layer of a silicon device. Mapping phase and amplitude information from the capacitance (dC/dV) signal identified locations of p- and n-type carriers and lossy regions as well as concentration of carriers at each point.

After these images obtained through constant external bias (or constant current), Dr. Chintala expanded his examples to those that included another measurement element:

5. DataCube SCM on PNP transistors
   To obtain a 3D cube of data (capacitance as a function of voltage at each location in the sample), the voltage is ramped at each point while the capacitance is measured. That data is stored in an array which can be resliced and analyzed for any relevant axis value. In this case, the data (from N. Chevalier and D. Mariolle of Uni. Grenoble Alpes, CEA, LETI, France) notably showed a defect only at certain applied voltages in PNP transistors.

   – Note: You can learn more about DataCube modes from our free E-Book that can be downloaded here.

6. C-AFM tomography of a conductive filament
   In AFM tomography, a very hard (e.g., diamond) probe is used to remove material from the surface with a larger force, then imaging on the newly-exposed surface occurs at a lower force. Repeating this removal-then-imaging cycle, a set of known-depth image slices are generated. Stacking of these image slices creates a tomographic dataset, as in the example shown of a conductive filament [6].

7. Photo-KPFM on organic materials
   Though the height and adhesion channels did not show a difference between the "light on" and "light off" conditions of an organic photovoltaic (sample courtesy of P. Leclère, University of Mons), the potential channel using Kelvin probe force microscopy (KPFM) did. When the light was switched on, the surface charged and the work function changed.

8. Dopant carrier profile for process monitoring
   A bonded device was cross sectioned, so that two samples could be scanned side by side. Dopant concentration was measured using scanning microwave impedance microscopy (sMIM) across the two samples. The plot of dopant concentration (data from PrimeNano Inc.) clearly showed different regions and made it straightforward to spot differences between the two samples.

Battery Technology

Dr. Guo presented several case studies looking into the individual components of lithium-ion batteries (LIB). He noted that since LIB are so well-developed and AFM is so versatile, there has been battery research done using a wide variety of AFM modes. Importantly, these measurements often take advantage of the adaptability of environmental conditions: in a glove box, in liquid, or at various temperatures.

1. Cathode electrical and mechanical property mapping
   DataCube tunneling AFM (TUNA) was used to test conductivity of a cathode sample under different voltages. Looking at different signal channels, the sample was mapped according to height, stiffness, modulus, and current. With the DataCube capability added in, an image could be extracted for discrete values within the voltage sweep (along the I-V curve).

2. SEI layers on graphitic electrodes
   In-situ solid electrolyte interface (SEI) layer growth was compared between two different graphitic materials using C-AFM [7]. The layer could be seen to grow during charging until reaching a relatively homogeneous state for the highly ordered pyroltic graphite. In contrast, the disordered graphite had preferential growth at the edges and less uniform defect shapes.

3. Microfabricated amorphous silicon anode
   Anodes are typically C-based, but an alternative with high capacitance is microfabricated Si-based anodes. This case study for C-AFM layered aluminum oxide (Al_2O_3) onto a Si-based anode and tracked topography and performance over several charging cycles [8]. Without the Al_2O_3 protective layer, there were significant changes in the topography and conductivity of the anode.

4. Ion and electron migration in composite solid-state electrolyte
   AFM was used to examine the mechanisms of ion and electron migration in a composite solid-state electrolyte at different temperatures and with varying amounts of Lithium lanthanum zirconium oxide (LLZO) [9]. With increasing temperature, modulus decreased and adhesion increased. At higher temperatures, the Poly(ethylene oxide) (PEO) deviated from its crystalline form (seen through topographical imaging). Conductivity measurements indicated that the PEO was only conductive in the high-temperature amorphous phase, and not in the lower-temperature crystalline phase.

FIGURE 4.

This sample is a metal oxide cathode measured with DataCube TUNA. Property maps shown are (left to right): height, modulus, and conductivity.

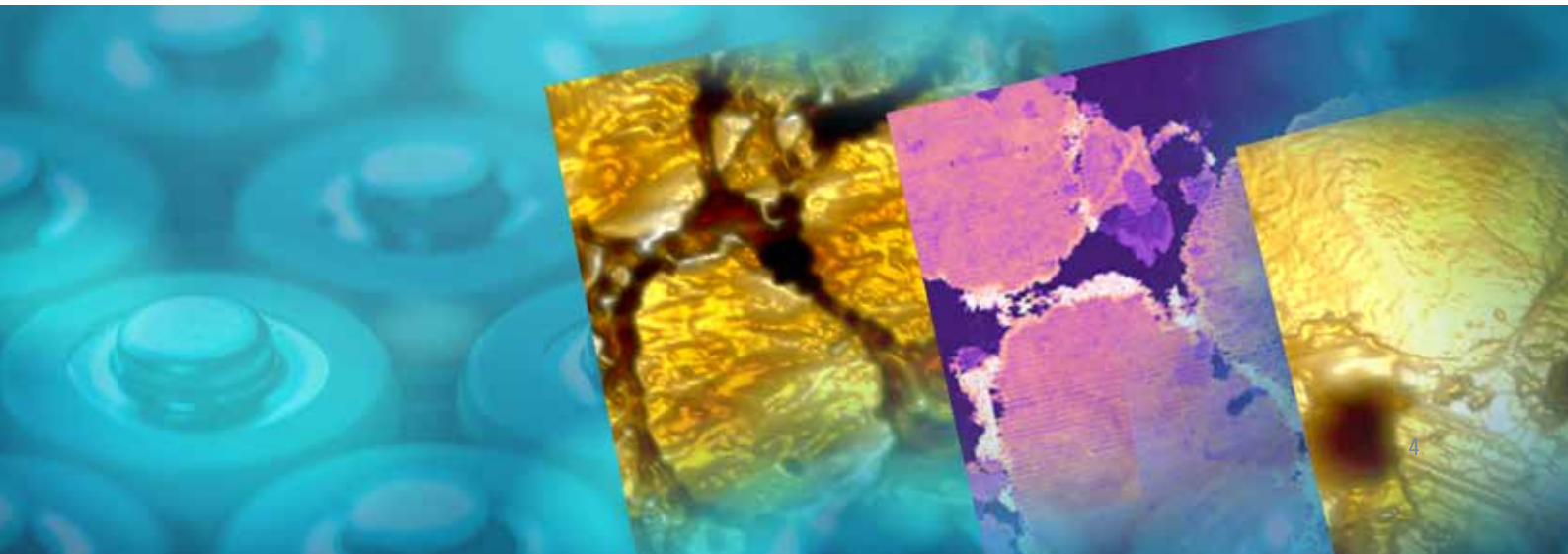

2D Materials

Dr. De Wolf presented the final six case studies, on the topic of 2D materials:

1. Epitaxial graphene on SiC
   A silicon carbide (SiC) sample was partially covered in graphene, with preferential coverage at the edges of the SiC steps (sample courtesy of R. Elmquist, NIST). Topography alone does not clearly show the location of graphene coverage, but it can be seen using adhesion, DMT modulus, surface potential, or phase mapping.

2. Suspended graphene membranes
   PeakForce Tapping was used to nondestructively image fragile suspended graphene membranes [10]. The very low imaging forces available in PeakForce Tapping mode made this imaging possible, where TappingMode was unsuccessful.

3. Programmable graphene nanobubbles
   A voltage was applied between tip and sample to desorb hydrogen on a germanium (Ge) substrate and form hydrogen gas nanobubbles [11]. This method can produce localized nanobubbles with incredible resolution and control.

4. Co-localized Raman and KPFM on graphene
   Topographical and KPFM imaging were performed on a multilayer graphene sample. Raman microscopy was carried out at the same location as the topographical and KPFM imaging (co-localized imaging). From the resulting correlated datasets, it was possible to distinguish each of the graphene layers and the properties of each successive layering.

5. Moiré pattern graphene on hBN
   Overlaid graphene and hexagonal boron nitride (hBN) with different respective orientations combine to produce different moiré patterns. The moiré pattern in different zones of the sample (corresponding to different orientations) was observed with sMIM (data provided by PrimeNano Inc.), and periodicity was measured, down to several nanometers.

6. Nanoscale redox mapping at the MoS_2-liquid interface
   In this study, single- and multilayer molybdenum disulfide (MoS_2) were placed in an electrochemical environment and measured using scanning electrochemical microscopy (SECM) and KPFM [12]. The resulting data showed that electrochemical activity scaled with layer thickness.

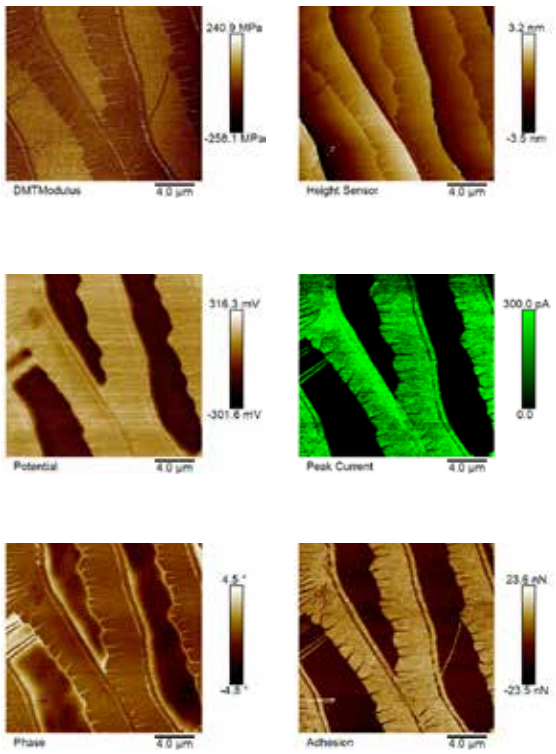

FIGURE 5.

Graphene grown epitaxially on SiC, mapped using PeakForce QNM, PeakForce KPFM™, and PeakForce TUNA.

FIGURE 6.

Co-localized mapping of graphene: height, Raman G-band, and Raman 2D-band (top to bottom).

Further Information

If you would like more information after watching the webinar, you can visit our website page describing the modes, or find probes to match your application. You can learn more about DataCube modes from our free E-Book that can be downloaded here.

References

[1] Pittenger, B., Osechinskiy, S., Yablon, D., and Mueller, T. (2019). Nanoscale DMA with the Atomic Force Microscope: A New Method for Measuring Viscoelastic Properties of Nanostructured Polymer Materials. *JOM*, 71(10), 3390–3398. https://doi.org/10.1007/s11837-019-03698-z

[2] Tang, F., Bao, P., Roy, A., Wang, Y., and Su, Z. (2018). In-situ spectroscopic and thermal analyses of phase domains in high-impact polypropylene. *Polymer*, 142, 155–163. https://doi.org/10.1016/j.polymer.2018.03.037

[3] Farrance, O. E., Jones, R. A. L., and Hobbs, J. K. (2009). The observation of rapid surface growth during the crystallization of polyhydroxybutyrate. *Polymer*, 50(15), 3730–3738. https://doi.org/10.1016/j.polymer.2009.05.061

[4] Hobbs, J. K., Farrance, O. E., and Kailas, L. (2009). How atomic force microscopy has contributed to our understanding of polymer crystallization. In *Polymer* (Vol. 50, Issue 18, pp. 4281–4292). Elsevier BV. https://doi.org/10.1016/j.polymer.2009.06.021

[5] Wang, B., Chen, J., Shen, C., Reiter, G., and Zhang, B. (2019). Relation Between Charge Transport and the Number of Interconnected Lamellar Poly(3-Hexylthiophene) Crystals. *Macromolecules*, 52(16), 6088–6096. https://doi.org/10.1021/acs.macromol.9b01146

[6] Celano, U., Goux, L., Belmonte, A., Opsomer, K., Franquet, A., Schulze, A., Detavernier, C., Richard, O., Bender, H., Jurczak, M., and Vandervorst, W. (2014). Three-Dimensional Observation of the Conductive Filament in Nanoscaled Resistive Memory Devices. *Nano Letters*, 14(5), 2401–2406. https://doi.org/10.1021/nl500049g

[7] Zhu, H., Russell, J. A., Fang, Z., Barnes, P., Li, L., Efaw, Corey, M., Muenzer, A., May, J., Hamal, K., Cheng, I. F., Davis, P. H., Dufek, Eric, J., and Xiong, H. (2021). A Comparison of Solid Electrolyte Interphase Formation and Evolution on Highly Oriented Pyrolytic and Disordered Graphite Negative Electrodes in Lithium-Ion Batteries. *Small*, 17(52), 2105292. https://doi.org/10.1002/smll.202105292

[8] Becker, C. R., Prokes, S. M., and Love, C. T. (2016). Enhanced Lithiation Cycle Stability of ALD-Coated Confined a-Si Microstructures Determined Using In Situ AFM. *ACS Applied Materials and Interfaces*, *8*(1), 530–537. https://doi.org/10.1021/acsami.5b09544

[9] Shen, C., Huang, Y., Yang, J., Chen, M., and Liu, Z. (2021). Unraveling the mechanism of ion and electron migration in composite solid-state electrolyte using conductive atomic force microscopy. *Energy Storage Materials, 39*, 271–277. https://doi.org/10.1016/j.ensm.2021.04.028

[10] Clark, N., Oikonomou, A., and Vijayaraghavan, A. (2013). Ultrafast quantitative nanomechanical mapping of suspended graphene. *Physica Status Solidi (b)*, *250*(12), 2672–2677. https://doi.org/10.1002/pssb.201300137

[11] Jia, P., Chen, W., Qiao, J., Zhang, M., Zheng, X., Xue, Z., Liang, R., Tian, C., He, L., Di, Z., and Wang, X. (2019). Programmable graphene nanobubbles with three-fold symmetric pseudo-magnetic fields. *Nature Communications*, 10(1), 3127. https://doi.org/10.1038/s41467-019-11038-7

[12] Du, H.Y., Huang, Y.F., Wong, D., Tseng, M.F., Lee, Y.H., Wang, C.H., Lin, C.L., Hoffmann, G., Chen, K.H., and Chen, L.C. (2021). Nanoscale redox mapping at the MoS_2-liquid interface. *Nature Communications*, 12(1), 1321. https://doi.org/10.1038/s41467-021-21660-z

©2023 Bruker Corporation. C-AFM, PeakForce KPFM, PeakForce QNM, PeakForce Tapping, PeakForce TUNA, and TappingMode are trademarks of Bruker. All other trademarks are the property of their respective companies. All rights reserved. AN157, Rev. A0.

Bruker Nano Surfaces and Metrology

Santa Barbara, CA • USA
Phone +1.805.967.1400

productinfo@bruker.com

www.bruker.com/AFMmodes